PHYSICAL REVIEW C VOLUME 18, NUMBER 3 SEPTEMBER 1978

Regge pole analysis of the scattering of ^{16}O by ^{28}Si

T. Takemasa* and T. Tamura
Department of Physics, University of Texas, Austin, Texas 78712
(Received 10 February 1978)

By using several optical potentials which fit satisfactorily results of a recent experiment on the elastic scattering of ^{16}O by ^{28}Si at $E_{lab} = 55$ MeV, exact calculations were performed so as to locate the positions of the Regge poles, and to evaluate the associated residues and corresponding background integrals. Based on the results thus obtained, a discussion is given of the roles which the pole and background terms play in the description of the scattering between two heavy ions.

[NUCLEAR REACTIONS Exact derivation of Regge poles; Residue; Pole and background decomposition of scattering amplitude; $^{16}O + ^{28}Si$ at $E_{lab} = 55$ MeV.]

I. INTRODUCTION

Recently Braun-Munzinger *et al.*[1] performed an experiment to study elastic and inelastic scattering of ^{16}O by ^{28}Si, observing the cross section out to 180°, and found that the cross sections at these angles are rather large and are highly oscillatory. Previously, the same cross section was measured up to about 60° and was analyzed by Cramer *et al.*,[2] who found that a potential which they call "E18" fits the limited data quite well. This potential belongs to the so-called strongly absorptive family. Braun-Munzinger *et al.*[1] found that the E18 potential gives too small cross sections at larger angles, where the experimental data can be fitted very well by a Legendre polynomial $|P_l(\cos\theta)|^2$, l being close to the grazing angular momentum l_g. They, therefore, added a term[3] with parameters such that this term resembles a contribution from a Regge pole, which causes phenomenologically a shape resonance at $l \approx l_g$.

What the data of Ref. 1 showed is that the optical potential to be used must have a character that is largely different from that of E18. Thus, a few groups of workers[4-6] undertook to search for such potentials. With such potentials one can fit the data rather well, if not perfectly, and thus there remains no need to add a Regge-pole type term in an *ad hoc* way.

It should be remarked that the Regge pole is something that can be derived, once a potential is given.[7] This was discussed for heavy-ion scattering in detail by Tamura and Wolter[8] (TW). With the new data of Ref. 1, and a renewed interest in the elastic scattering between heavy ions, we have taken up this problem once again. Through accurate calculations to locate the Regge poles, the major portion of the present paper is devoted to the numerical study of the role of the pole and background terms in the Regge description of heavy-ion elastic scattering. In performing calculations, four sets of optical potential parameters were considered; first E18[2] and then those by Shkolnik and Dehnhard (SD),[4] Golin and Kahana (GK),[5] and Lee and Chan (LC).[6]

The present work can be considered an extension and/or continuation of our previous work.[8] The basic formulas used here are essentially the same as those that appeared in TW. We thus give in Sec. II only a very few, those which are needed in making clear the explanation of the results of the calculations. The method of numerical calculations are the same as in TW, and we shall not repeat any discussion of it here. In TW, discussions were given about the general behavior of the Regge poles and the associated background integrals. In particular we discussed in considerable detail the energy dependence of the Regge poles, i.e., the behavior of the Regge trajectories. We also discussed their dependence on the choice of colliding partners. In the present paper, we concentrate our attention, on the contrary, to one pair, colliding with a fixed energy; the elastic scattering of ^{16}O by ^{28}Si with $E_{lab} = 55$ MeV.[1] In Sec. III, the results of the calculation are presented. The summary of our results and discussion are given in Sec. IV.

II. SUMMARY OF THE FORMULAS

In the present section we give several formulas which are needed for explaining the results of our numerical calculations, as given in the next section. These formulas are essentially the same as some of those that appeared in TW. We shall thus give them here without discussing their derivation.

The amplitude for elastic scattering between two spinless particles can be written as

$$f(\theta) = f_c(\theta) + \frac{1}{k}\sum_{l=0}^{\infty}(2l+1)e^{2i\sigma_l}C_l P_l(\cos\theta), \qquad (1)$$

where $f_c(\theta)$ is the Rutherford scattering amplitude. Other notation is standard except that C_l is the partial wave amplitude, related to the nuclear S-matrix element S_l by

$$C_l = \frac{1}{2i}(S_l - 1). \tag{2}$$

In the next section, we use mostly the Regge representation, in which C_l is expressed as[9]

$$C_l = \sum_n \frac{2\lambda_n}{\lambda^2 - \lambda_n^2}\beta_n + \frac{1}{2\pi i}\int_c d\lambda' \frac{2\lambda' C(\lambda')}{\lambda^2 - \lambda'^2}, \quad \lambda = l + \tfrac{1}{2}. \tag{3}$$

Here $C(\lambda)$ is defined by the analytic continuation of C_l into the complex λ plane, and the contour c is taken along a path so that $\mathrm{Re}\,\lambda' \to \infty$. In the first term of Eq. (3), λ_n is the position of the Regge pole, while β_n is the residue of $C(\lambda)$ at $\lambda = \lambda_n$. The summation is taken over all the Regge poles that lie inside the contour c. The position of λ_n is of course defined as a point in the λ space at which the $C(\lambda)$ coefficient, corresponding to the Schrödinger equation

$$\left(-\frac{\hbar^2}{2\mu}\frac{d^2}{dr^2} + \frac{\hbar^2}{2\mu}\frac{\lambda^2 - \frac{1}{4}}{r^2} + V(r) - E\right)\psi(\lambda, E, r) = 0, \tag{4}$$

becomes singular. This definition can also be rephrased by saying that the regular solution $\psi(\lambda, E, r)$ of Eq. (4) is smoothly matched into the asymptotic form that consists purely of an outgoing Coulomb wave function.[7]

In Sec. III, we also use briefly the Δ representation.[8] This means that we express C_l as

$$C_l = \sum_n \frac{\beta_n F(\lambda, \lambda_n)}{\lambda - \lambda_n} + \sum_m \frac{\gamma_m C(\lambda_m)}{\lambda - \lambda_m} + \frac{1}{2\pi i}\int_c d\lambda' \frac{C(\lambda')F(\lambda, \lambda')}{\lambda - \lambda'}, \tag{5}$$

with

$$F(\lambda, \lambda') = 2/\{1 + \cosh[(\lambda - \lambda')/\Delta]\}. \tag{6}$$

Because of the exponential dependence of $F(\lambda, \lambda')$ on $|\lambda - \lambda'|$, the contribution of the pole λ_n is localized to the l values for which $|\lambda - \lambda'|$ is small. On the other hand, the pole term decreases only as λ^{-2} on both sides of the pole λ_n, if the Regge representation (3), which can also be obtained from Eq. (5) by setting $F(\lambda, \lambda') = 2\lambda'/(\lambda + \lambda')$, is employed. In the second term of Eq. (5), λ_m is the pole of $F(\lambda, \lambda')$, considered as a function of λ' for the fixed λ and γ_m is the corresponding residue. This pole does not play any significant role in the discussion of Sec. III.

In Sec. III, we discuss the separate contributions of the pole and the background integral to C_l, and for that purpose we divide C_l into two parts as

$$C_l = C_l^P + C_l^B. \tag{7}$$

Here the pole term C_l^P denotes the first term of either Eq. (3) or Eq. (5), while the background term C_l^B includes the rest. Note that how many poles are included in C_l^P depends on the choice of the contour c. We may use the notation, e.g., C_l^P $(n = 0\text{–}3)$ to mean that the first four poles are taken into account in C_l^P. (How to number the poles is discussed in Sec. III.)

In Sec. III, we also present cross sections denoted by σ_P, σ_B, and σ_T. Here σ_P, which may be called the cross section with the pole term only, is obtained from Eq. (1) by replacing C_l there by C_l^P, and further suppressing $f_c(\theta)$. On the other hand σ_B, which may be called the cross section with the background term only, is obtained from Eq. (1) by using C_l^B in place of C_l and retaining $f_c(\theta)$. Finally, σ_T (the suffix T standing for total) is the cross section in which both the pole and background contributions are taken into account. By construction, this is nothing but the cross section that is obtained by using Eq. (1) as it stands, and agrees exactly with the cross section that is obtained in the usual optical model calculation.

III. RESULTS OF CALCULATIONS

A. Behavior of the Regge poles

As we remarked in the Introduction, we consider four potentials[2,4–6] in the present work and the parameters for these potentials are summarized in Table I. It should be noted that, except for the E18 potential,[2] all the parameters were taken from unpublished sources. The authors of Refs. 4–6 very generously supplied us with this information. The parameters listed in Table I were the best set these authors had found by the time they were given to us. Therefore, they should not be taken as the best set which these authors will eventually obtain within the framework of their search. We therefore specifically want to avoid any comparison of the relative merits of these potentials concerning the fitting of the data of Ref. 1. As far as the parameters given in Table I are concerned, the LC potential[6] fits experiment best, but the other two[4,5] also fit the data fairly well, and we may say that all of these three potentials are realistic. The situation can be seen from Fig. 1 in which the experimental data[1] are plotted together with the predictions of the SD,[4] GK,[5] and LC[6] potentials. As was shown in Ref. 1, however, the E18 potential does not fit the data, unless a Regge pole term is added in an *ad hoc* fashion.

A characteristic feature of the E18 potential is that it is strongly absorptive and has a rather shallow real part. Both SD[4] and GK[5] potentials are

TABLE I. Optical model parameters used in the calculation. The E18, SD, and GK potentials are of standard Woods-Saxon form, and their parameters are given in the table with well known notation. The LC potential is given by

$$V(r) = (286.5 + i19.7) \times \{1 + 0.99\exp[(r-R)/3.70] + \exp[(r-R)/0.49]\}^{-1}$$

with $R = 1.122 \times (A_1^{1/3} + A_2^{1/3})$ and $r_c = 1.2$ fm.

Label	V_0 (MeV)	r_0 (fm)	a_0 (fm)	W_0 (MeV)	r_I (fm)	a_I (fm)	r_c (fm)	Ref.
E18	10.0	1.35	0.618	23.4	1.23	0.552	1.0	2
SD	27.456	1.310	0.485	4.865	1.277	0.323	1.0	4
GK	75.2133	1.2355	0.4929	8.5	1.2065	0.1844	1.4204	5

surface transparent, and the former (latter) has a shallow (deep) real part. The LC[6] potential has a geometry, common to its real and imaginary parts, which is not of a Woods-Saxon form. As is seen from the formula given in the caption of Table I, its denominator has two exponents. Another characteristic feature of the LC potential is that its real part is very deep and the imaginary part is also fairly strong.

Figure 2 shows the locations of the Regge poles, in the first quadrant of the complex λ plane, obtained for these four potentials by performing rigorous calculations as explained in TW. For Re $\lambda > 0$ and positive energy no Regge poles can occur in the domain Im $\lambda \leq 0$,[7] if the spin-orbit potential is not taken into account as is the case here. Thus it is sufficient to search for Regge poles only in the first quadrant in the λ plane. Search for poles was made within the rectangle with Re $\lambda = 0 \sim 45$ and Im $\lambda = 0 \sim 7$, where $\lambda = \text{Re}\,\lambda + i\,\text{Im}\,\lambda$. There are no poles within this rectangle other than those shown in Fig. 2.

This figure alone already tells us a good deal about the differences and/or similarities of the behavior of these potentials. One thing to be noted at first is that the E18 potential has one and only one Regge pole. On the other hand, the LC, GK,

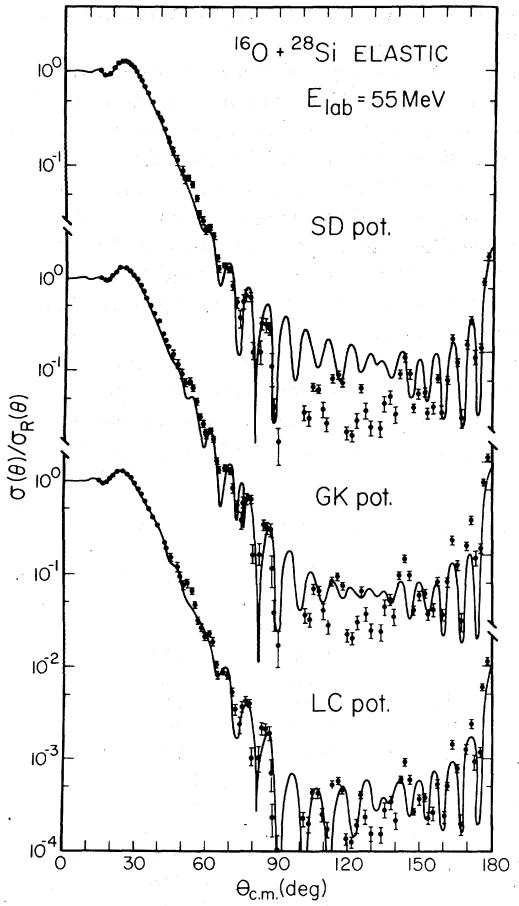

FIG. 1. Comparison of the optical model calculations using the SD, GK, and LC potentials with the experimental cross sections.

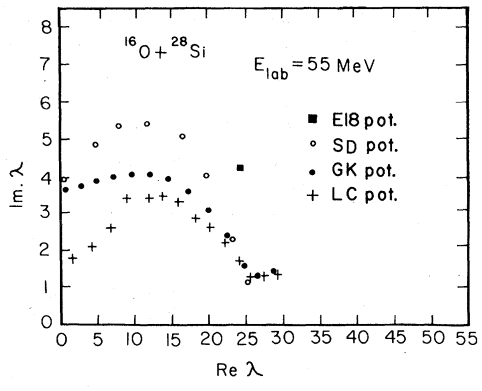

FIG. 2. Positions of Regge poles in the first quadrant of the complex λ plane for the elastic scattering of ^{16}O by ^{28}Si at $E_{lab} = 55$ MeV for several potentials.

and SD potentials have, respectively, 14, 13, and 8 Regge poles. It will be recognized that the number of poles is roughly proportional to the depth of the real potential. We may say that, in this regard, the GK and LC potentials share a strong similarity.

The positions of these Regge poles, and their associated residues β_n, are given in Tables II–V for the four potentials. The poles are labeled as $n=0,1,2\cdots$, according to the decreasing order of the value of Re λ. Note that for the $n=0$ and $n=1$ poles of the LC potential and for the $n=0$ pole of the GK potential, the values of $|\beta_n|$ are extremely small. It should also be noted that $|\beta_7|$ of SD and $|\beta_{12}|$ of the GK potentials are anomalously large. The origin of these large values may be the following.

As is seen in Tables III and IV, these poles have Re $\lambda \approx 0$ and Im $\lambda \neq 0$. For a complex λ, the centrifugal potential is written as

$$\frac{\hbar^2}{2\mu}\frac{\lambda^2-\frac{1}{4}}{r^2}=\frac{\hbar^2}{2\mu}\frac{(\mathrm{Re}\,\lambda)^2-(\mathrm{Im}\,\lambda)^2-\frac{1}{4}}{r^2}+2i\frac{\hbar^2}{2\mu}\frac{(\mathrm{Re}\,\lambda)(\mathrm{Im}\,\lambda)}{r^2}, \tag{8}$$

which is reduced to

$$\frac{\hbar^2}{2\mu}\frac{\lambda^2-\frac{1}{4}}{r^2}=-\frac{\hbar^2}{2\mu}\frac{(\mathrm{Im}\,\lambda)^2+\frac{1}{4}}{r^2}, \tag{9}$$

if Re $\lambda = 0$. Therefore, the centrifugal potential with Re $\lambda \approx 0$ tends to become a singular attractive potential. This would make the corresponding $|\beta_n|$ anomalously large. We note further that the LC potential does not have a pole close to the imaginary axis, and thus has no anomalous β_n.

It is instructive to present, for some values of λ, the potential $V_{\mathrm{eff}}(r)$ and the corresponding wave function $\psi(\lambda, E, r)$ of Eq. (4) plotted as functions of the radius r. Here the effective potential $V_{\mathrm{eff}}(r)$ is the sum of the optical potential $V(r)$, which includes the Coulomb potential, and the centrifugal potential. As is seen in Eq. (8), the imaginary part of the centrifugal potential is positive definite (or non-negative definite to be more precise) in the first quadrant. Therefore, it plays the role of a source, unlike the imaginary part of the optical potential, which works as a sink.

In making this presentation, we chose the SD potential for no specific reason. The potentials for selected λ values are displayed in the lower parts of Figs. 3–5 and the wave functions corresponding to these potentials in the upper parts. The center of mass (c.m.) energy $E_{\mathrm{c.m.}}$ is also shown in each figure. Figures 3 and 4, respectively, correspond to the $n=3$ and $n=6$ Regge poles. On the other hand, the case shown in Fig. 5 does not correspond to a Regge pole, but to a real λ whose value equals the grazing angular momentum $\lambda=\lambda_g=24.5$.

There are a number of Regge poles for the SD, GK, and LC potentials, which have fairly large, but not anomalously large, values for β_n, and we may call them "standard" Regge poles. The shape of the potential and of the corresponding wave function belonging to these poles are rather similar to one another, in their characteristic behavior. Therefore, those presented in Fig. 3 for the $n=3$ pole of SD can be considered to represent the behavior of most such poles.

The $n=3$ pole has $\lambda = 15.58 + i5.10$, as is seen in Table III. In other words, $(\mathrm{Re}\,\lambda)^2 \gg (\mathrm{Im}\,\lambda)^2$ there. This fact makes the behavior of the (real part of the) centrifugal potential much the same as that

TABLE II. The positions and the residues of the Regge poles for the elastic scattering of ^{16}O by ^{28}Si. The E18 potential is used.

n	Reλ_n	Imλ_n	Reβ_n	Imβ_n
0	24.29	4.20	1.773	0.667

TABLE III. Same as Table II except that the SD potential is used.

n	Reλ_n	Imλ_n	Reβ_n	Imβ_n
0	25.30	1.17	0.241	0.198
1	23.05	2.27	1.135	1.353
2	19.61	4.05	2.216	−1.732
3	15.58	5.10	−2.891	−0.092
4	11.63	5.44	4.067	1.250
5	8.01	5.36	−7.026	−9.934
6	4.88	4.89	−35.358	24.621
7	0.14	3.89	−55.732	369.174

TABLE IV. Same as Table II except that the GK potential is used.

n	Reλ_n	Imλ_n	Reβ_n	Imβ_n
0	28.89	1.46	0.002	−0.002
1	26.50	1.29	0.125	0.029
2	24.67	1.58	0.312	0.739
3	22.44	2.39	1.089	1.234
4	19.91	3.06	2.691	−0.606
5	17.28	3.56	−0.444	−4.021
6	14.63	3.90	−5.599	1.272
7	11.98	4.07	3.024	7.524
8	9.44	4.07	9.466	−5.858
9	7.05	3.98	−11.140	−13.363
10	4.81	3.87	−28.013	18.972
11	2.64	3.74	0.436	81.375
12	0.52	3.62	60.961	221.667

TABLE V. Same as Table II except that the LC potential is used.

n	Reλ_n	Imλ_n	Reβ_n	Imβ_n
0	29.25	1.41	0.001	−0.001
1	27.31	1.34	0.032	0.004
2	25.64	1.33	0.167	0.258
3	24.00	1.72	0.175	0.840
4	22.10	2.21	0.992	1.277
5	20.07	2.632	2.748	0.044
6	17.98	2.99	1.629	−3.869
7	15.86	3.30	−5.177	−3.102
8	13.79	3.54	−3.129	7.127
9	11.67	3.41	6.077	2.780
10	9.06	3.44	5.276	−3.309
11	7.07	2.64	−0.653	−2.154
12	4.24	2.07	0.064	−0.901
13	1.77	1.80	0.314	−0.627

for a purely real λ. As is seen in Fig. 3, it in fact creates a centrifugal barrier, making the wave function very small for $r < 4$ fm. Note that for a value of λ that corresponds to a Regge pole, the asymptotic form of the wave function is a purely outgoing Coulomb wave function (cf. Sec. II), and the real and imaginary parts of this wave function plotted against r must be completely out of phase with one another. It is seen that the wave function shown in Fig. 3 does embody this fact for $r > 5$ fm. The envelope of the wave function increases (almost) monotonously in going from the internal to the asymptotic region. It is further seen in Fig. 3, that the real potential has a "trapping region" in the neighborhood of the surface, a fact which would encourage one to make a statement that the Regge pole describes the onset of a (single-particle type) resonance. This statement is, however, only half true. An outstanding counter example is the Regge pole for the E18 potential. As is seen from Table II, this pole is of the standard type, but it does not result from any trapping potential at the pole position. The behavior of the E18 Regge pole will be discussed further in Sec. C below.

The $n = 6$ pole is somewhat anomalous as listed in Table III. As is seen in Fig. 4, the real part of the potential is indeed singular and attractive at $r = 0$. On the other hand, the imaginary part is singular and positive at $r = 0$. In the region in which $r \geq 2.5$ fm, both the strength of the real and imaginary parts is rather small compared with $E_{\text{c.m.}} = 35$ MeV, and in this whole region the wave functions are very close to their asymptotic forms.

Finally the behavior of the potential and the wave function which we have for a real λ is presented by Fig. 5. As is seen, the real and imaginary parts of the asymptotic wave function are not mutually out of phase but almost in phase, contrary to the situation we encountered in Figs. 3 and 4. This in-phase feature is due to fact that the strength of the imaginary part of the optical potential is very weak compared with that of the real part. See the lower part of Fig. 5. They thus have both an incoming, as well as an outgoing, Coulomb wave function in the asymptotic region. It is well known[7] that for $E > 0$ and Re $\lambda > 0$ there is no Regge pole on the real axis.

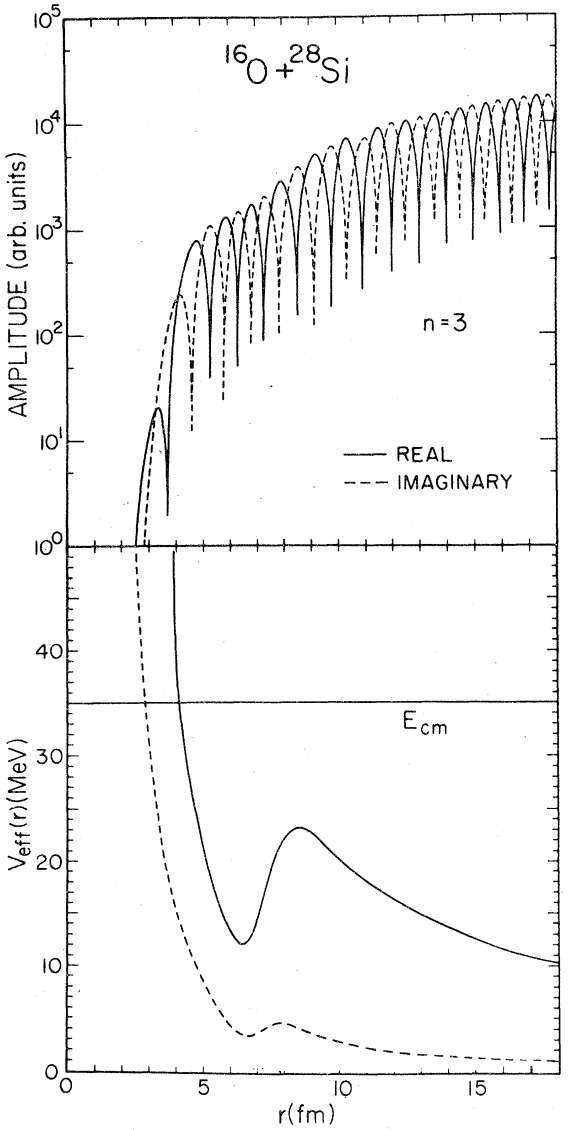

FIG. 3. (Top) The amplitude of the $n = 3$ pole wave in the SD potential. (Bottom) The real and imaginary parts of $V_{\text{eff}}(r)$ at the $n = 3$ pole. They are shown as functions of the radius r.

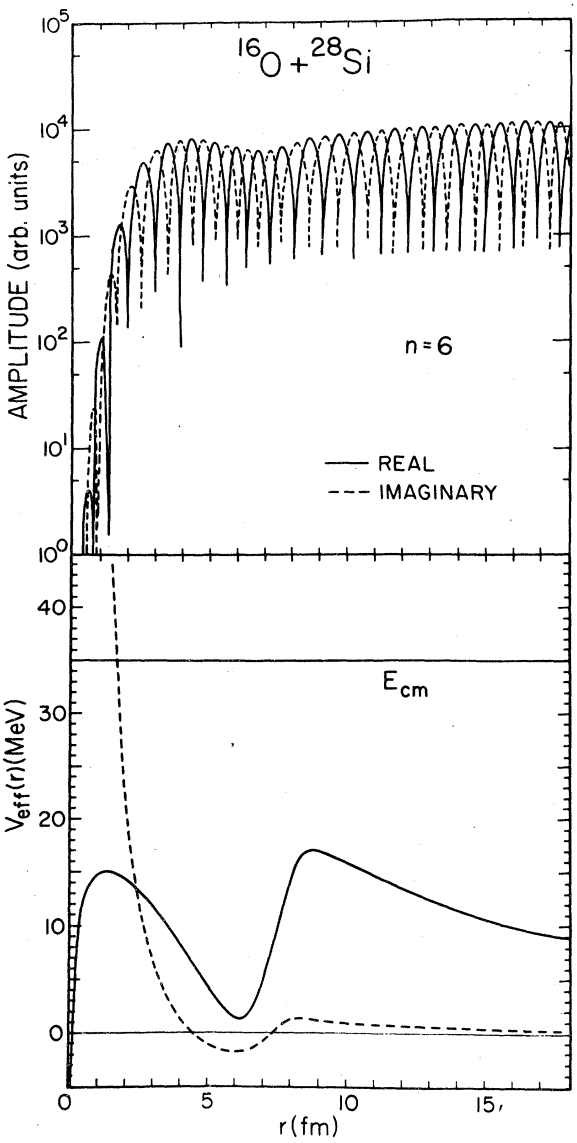

FIG. 4. Same as Fig. 3 except that it is for the case of the $n=6$ pole.

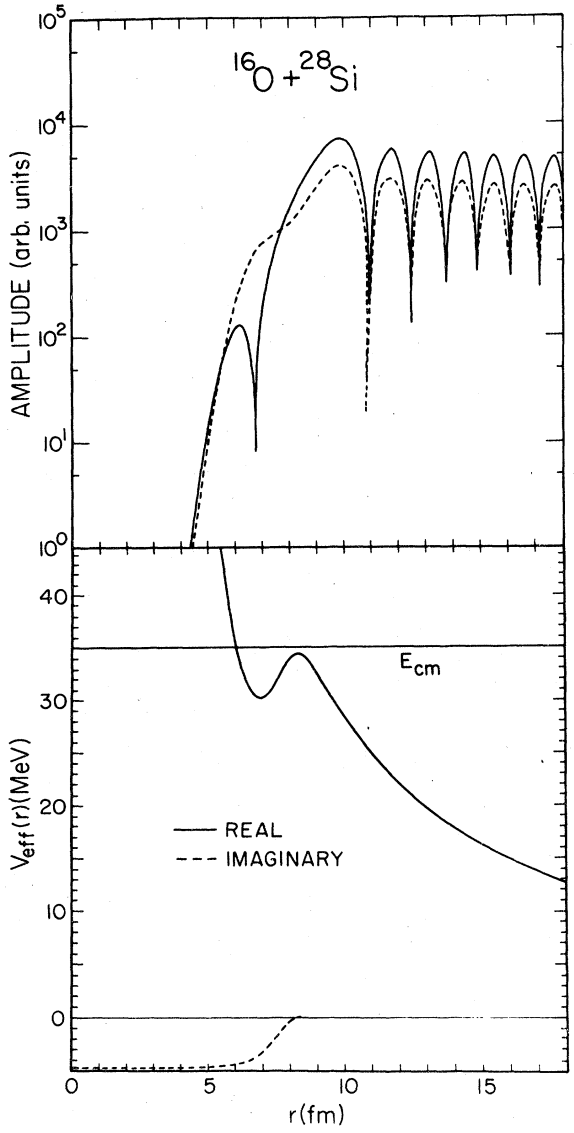

FIG. 5. Same as Fig. 3 except that it is for the case of the grazing angular momentum $\lambda_g = 24.5$.

B. Pole and background contributions to partial wave amplitudes

In Fig. 5, we plot the three terms $|C_l^P|$, $|C_l^B|$, and $|C_l|$ in Eq. (7) as functions of l to study the contributions of the pole and background terms to the partial wave amplitude. We chose, as an example, the LC potential here, which has 14 Regge poles. Figure 6 actually consists of 14 smaller figures, and in the one denoted as $n=0$, only the $n=0$ pole contribution is taken into account in C_l^P, i.e., in the first term of Eq. (3). In the next figure, which is denoted as $n=0$–1, the contributions of the $n=0$ and $n=1$ poles are taken into account, and so on. In the following discussions, the Regge representation of Eq. (3) will be used unless stated otherwise.

In the $n=0$, and $n=0$–1 cases, $|C_l^P|$ is very small because the residues corresponding to the $n=0$ and $n=1$ poles are extremely small. Therefore, we have $|C_l^B| \approx |C_l|$. By the time we come to $n=0$–3, however, $|C_l^P|$ acquires a significant value, and at $n=0$–4, it begins to predominate $|C_l^B|$, at least for l's that are close to the grazing value. It should be also noted that the peak of $|C_l^P|$ moves toward the lower l values when the number of the poles considered increases. This is due to the fact that $|\beta_n|$ becomes large with increased n.

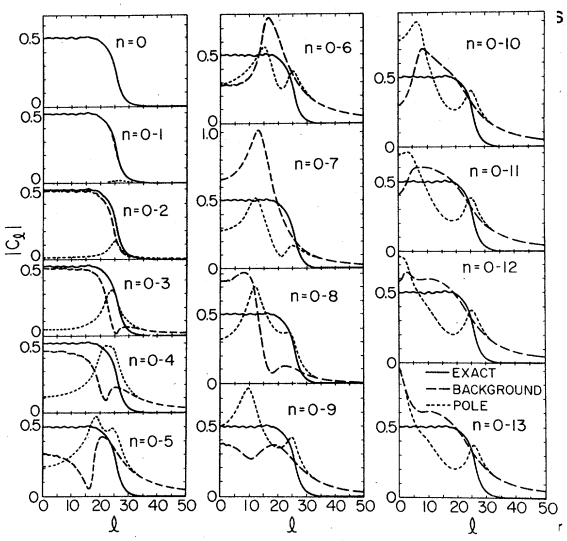

FIG. 6. Moduli of C_l^P, C_l^B, and C_l for the LC potential in the Regge representation are plotted as functions of l. The notation $n=0-2$, e.g., means that the contributions of the $n=0$, 1, and 2 poles are taken into account in the calculations of the C_l^P and C_l^B terms. The partial wave amplitude C_l is given by $C_l = C_l^P + C_l^B$.

With increasing number of poles, $|C_l^P|$ keeps increasing. The peak moves to lower l values and moreover it splits into two parts at $n=0-5$. However, this increase of $|C_l^P|$ does not take place at the expense of $|C_l^B|$; $|C_l^B|$ also increases in the region where $|C_l^P|$ has a peak, as is seen, e.g., in the $n=0-5$ or $n=0-6$ cases. The increase of $|C_l^B|$ is indeed needed, in order to keep $C_l = C_l^P + C_l^B$ independent of the number of poles considered in C_l^B. When the number of poles is further increased, the behavior of both C_l^P and C_l^B gets more and more erratic.

In obtaining $|C_l^B|$ plotted in Fig. 6, we performed the contour integral numerically, as it is defined in the second term of Eq. (3). Actually, such a calculation was unnecessary, because C_l can be obtained easily by the usual optical model calculation, and we can get C_l^B by subtracting C_l^P from C_l. We nevertheless carried out such calculations, because it served, by confirming that the calculated $C_l^P + C_l^B$ did agree with the optical model C_l, to confirm the accuracy of our calculations. It also guarantees that we have not overlooked any Regge pole inside the area enclosed by the contour chosen separately for each choice of the number of Regge poles in C_l^P. The actual shapes of the contours that are in fact used are shown in Fig. 7, for several choices of number of Regge poles.

Before discussing further the behavior of C_l^P and C_l^B given in Fig. 6, we present in Fig. 8 the cross sections σ_P, σ_B, and σ_T, calculated by using the

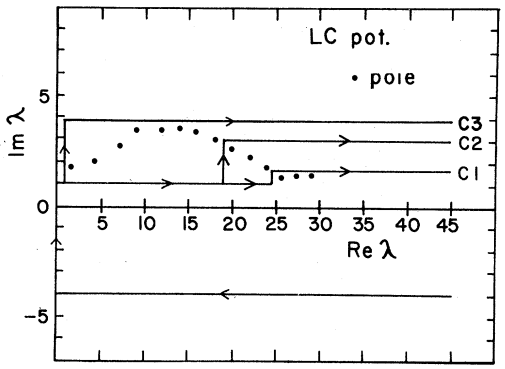

FIG. 7. The integration paths C_1, C_2, and C_3 in the λ plane used in the calculations of the background term C_l^B are shown for the cases of $n=0-2$, $n=0-5$, and $n=0-13$, respectively. Similar paths are used for other cases too.

LC potential, and making three different choices of the number of the poles $n=0-2$, $n=0-5$, and $n=0-13$. In these three cases presented in Fig. 8, the same total cross section σ_T is repeated, and is compared with experiment in Fig. 8(c).

In the case with $n=0-2$, we first note that, since $|\beta_0|$ and $|\beta_1|$ are very small, σ_P is dominated by a single pole $n=2$. In other words, this σ_P may be called the cross section obtained by making a "single-pole" approximation. Since it is seen that

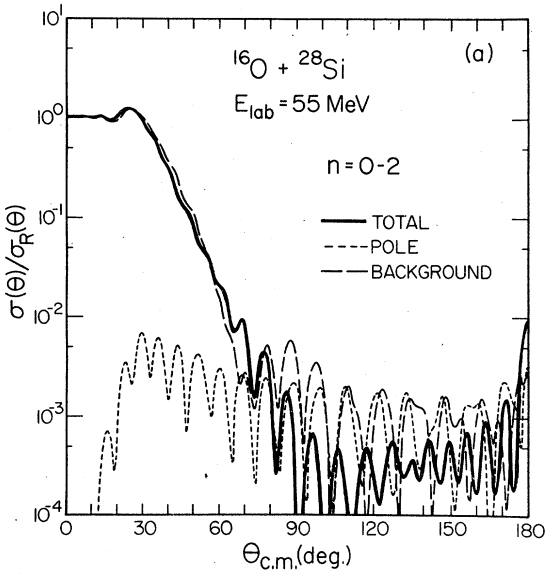

FIG. 8. Pole and background decomposition of the angular distribution in the LC potential in the Regge representation. The solid line is the total angular distribution which is obtained from the coherent superposition of the pole (short dashed line) and background (long dashed line) terms. The figures (a), (b), and (c) correspond to the cases in which the $n=0-2$, $n=0-5$, and $n=0-13$ are taken into account, respectively.

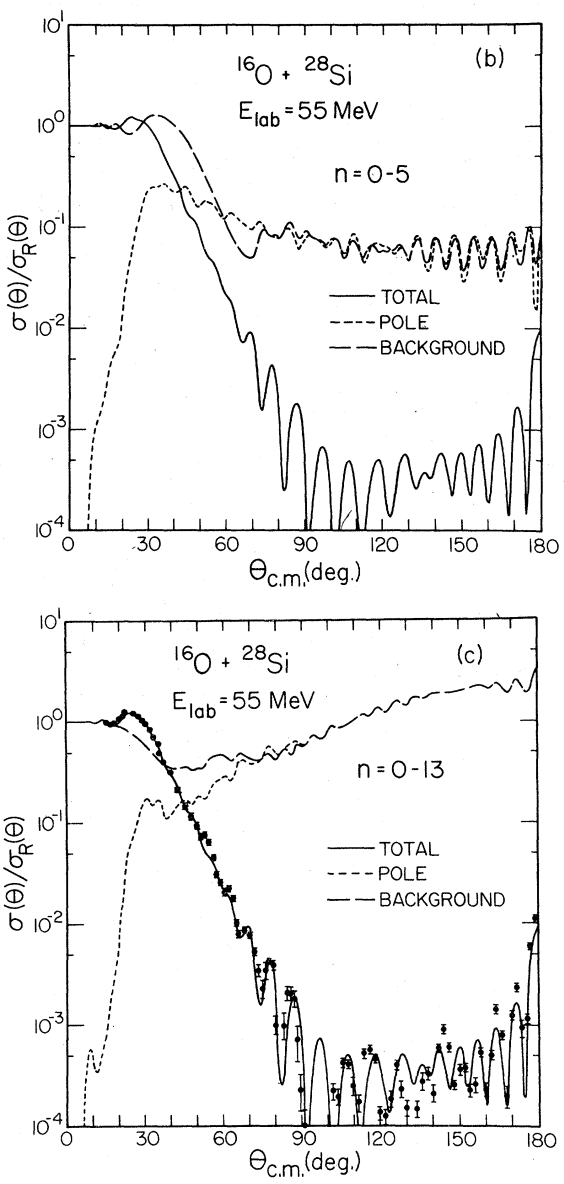

FIG. 8. *(Continued).*

this σ_P behaves in a way rather close to σ_T (and thus to σ_{exp}), one might tend to conclude that the back-angle cross section is accounted for by considering *one* Regge pole. Obviously, however, such a conclusion is true only when σ_B is very small in this angular region. As is seen in Fig. 8(a), σ_B actually has a similar magnitude as does σ_P at large angles, and its behavior is surprisingly close to that of σ_P. [Note that the apparent difference between σ_P and σ_B at smaller angles is largely due to the fact that σ_B includes the Coulomb amplitude $f_c(\theta)$, while σ_P does not, because of the definition made in Sec. II. This remark applies to Figs. 8(b) and 8(c), too.] This fact indicates that there exists a very delicate phase relation between C_l^P and C_l^B so that their superposed contribution ends up as σ_T.

We saw in Fig. 6 that, as the number of poles included in C_l^P increases, both $|C_l^P|$ and $|C_l^B|$ increase and take shapes similar to each other. It seems that this fact is reflected in the behavior of σ_P and σ_B, which is given in Fig. 8(b) for the case of $n = 0-5$. As is seen, they again behave very closely together, both now having magnitudes that are much larger than that of σ_T except at foward angles. It is thus clear that very strong destructive interference is taking place between C_l^P and C_l^B.

This strong cancellation between C_l^P and C_l^B is brought to its extreme when we come to the $n = 0-13$ case. As is seen in Fig. 8(c), both σ_P and σ_B are about four orders of magnitude larger than is σ_T. A fact which may be more surprising than the onset of this strong cancellation is that σ_P, as well as σ_B, lies very close to the Rutherford cross section σ_{Ruth} except at the forward angles. Note that in Fig. 8 various cross sections divided by σ_{Ruth} are plotted.

Summarizing, what we found in Fig. 8 is a very strong parallelism between σ_P and σ_B, and thus failure in singling out the effect of a particular Regge pole. Note that we have been using the Regge representation exclusively so far. We have emphasized in Sec. II that the Regge representation does not localize the contribution of a pole term C_l^P to a narrow region of the l values. One may thus suspect that our failure to single out the effect of one pole or two poles is due to the use of this representation. In order to see whether such a suspicion is correct or not, we repeated calculations by using the Δ representation, i.e., by using Eqs. (5) and (6). The parameter Δ which defines a width in the l space is taken to be $\Delta = 1.8$. The results are not sensitive to the value of Δ used.

In the inset of Fig. 8, we plot, as an example, $|C_l^P|$ and $|C_l^B|$ as functions of l in the case of $n = 0-3$. Thus this figure is to be compared with Fig. 6. It is seen that $|C_l^P|$ in the Δ representation is now strongly concentrated in the neighborhood of $l = 24$. This peak value of l is very close to 24.00 which is the Re λ value of the $n = 3$ pole. And in the region of $l \geq 24$, $|C_l^P|$ by itself almost reproduces the partial wave amplitude $|C_l|$. It thus seems that we have achieved the singling out of the $n = 3$ pole contribution. However, it is seen in Fig. 9, where σ_P and σ_B calculated by using these C_l^P and C_l^B are plotted, that the pole and background terms also interfere strongly with each other except at most backward angles. We found that their behavior is not very much different from what we obtained for

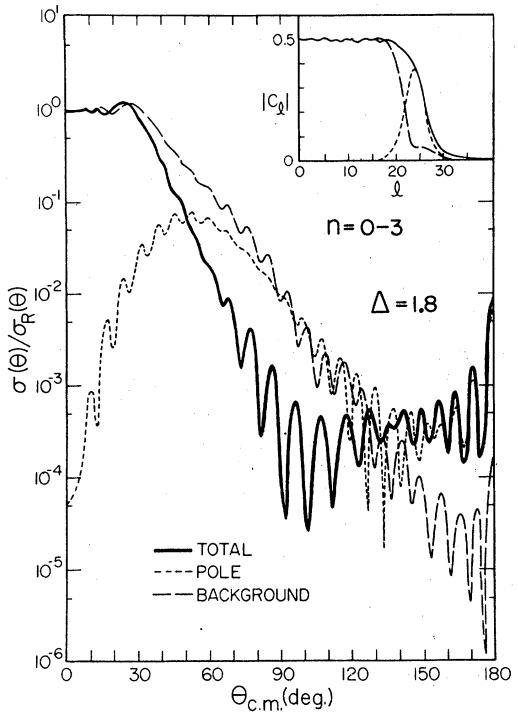

FIG. 9. Pole and background decomposition of the angular distribution in the LC potential in the Δ representation for the elastic scattering ^{16}O by ^{28}Si at $E_{lab} = 55$ MeV, in which the poles of $n = 0$–3 are taken in account.

$n = 0$–3 with the Regge representation. In other words, we are led to the conclusion that the use of the Δ representation does not result in the singling out of a pole, as one might have naively expected.

In concluding this section, we want to make a remark about recent work of Brink and his co-workers.[10,11] They analyzed the α-^{16}O and α-^{40}Ca scattering data in terms of a semiclassical method, and came to the conclusion that the large and highly oscillatory back-angle cross sections must be interpreted as a nuclear glory. When the semiclassical method is used, it is possible to separate the scattering amplitude into two parts, one reflected from the outermost turning point, and the other from the innermost turning point. They further showed that the former (latter) is responsible to the forward (backward) cross section. Note that the LC potential[6] was derived having in mind the results of this work.

From the fact that there are many Regge poles with lower values of Re λ, as is seen in Fig. 2, one might expect that C_l^P, which includes only poles with these lower Re λ, might resemble the amplitude corresponding to the reflection from the innermost turning point, because the latter certainly includes the contribution of lower partial waves. It turned out, however, that such is not the case. The very strong parallelism between the pole and background terms, as we emphasized above, seems to prevent this.

Finally, we want to stress that this very strong parallelism obtained in this subsection is not peculiar to the LC potential; all other potentials considered in the present work also show that one cannot single out the contribution of one or two pole terms which may reproduce by itself the angular distribution at the backward angles. As an example, we present in Fig. 10 the cross sections σ_P, σ_B, and σ_T in the case of $n = 0$, calculated by using the SD potential. Note that the contributions from the pole and background terms to the total angular distirubtion are very similar to those in the case of Fig. 8(a). Contrary to the present result, TW[8] found that in the case of the $^{16}O + ^{16}O$ elastic scattering at high $E_{c.m.}$, there are one or two poles which contribute dominantly to the cross sections at large angles. This difference may be attributed to the difference in the optical potentials used. TW used a potential whose real part has a strength which was much weaker than those used in the present study.

C. Regge poles associated with E18 potential

As remarked in the Introduction, Braun-Munzinger *et al.*[1] modified the S matrix generated by the E18 potential, which is strongly absorptive and has a very shallow real depth, by adding a Regge-pole type term[3] with parameters. Then they found

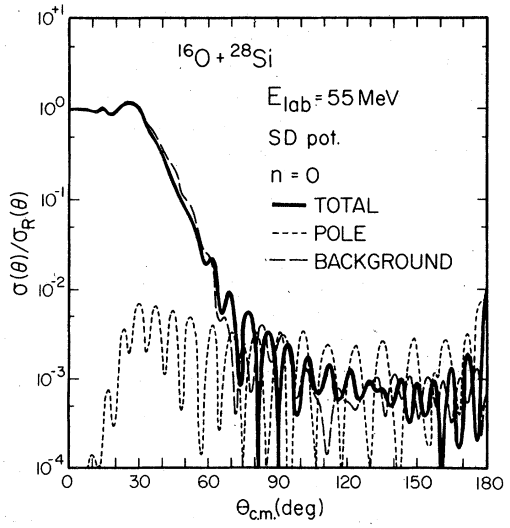

FIG. 10. Pole and background decomposition of the angular distribution in the SD potential in the Regge representation. The solid line is the total angular distribution which is obtained from the coherent superposition of the pole (short dashed line) and background (long dashed line) terms.

that this Regge-pole parametrization method reproduced fairly well the experimental data. It would thus be of some interest to see briefly the behavior of the Regge-pole term derived from the exact calculation and from the parametrization method.

In Fig. 2 and Table I, we showed that the E18 potential does have a Regge pole of its own. The real part of this Regge pole is nearly equal to the grazing value l_g but its imaginary part is fairly large compared with the poles of the other potentials which appeared in the $l \approx l_g$ region. This large Im λ causes the pole not to have the property of a resonance in the usual sense. It should be also noted that the E18 potential does not have a pocket in $V_{\text{eff}}(r)$, when λ takes the value of the pole position. In other words, an internal wave function that is matched smoothly into a purely outgoing Coulomb function can be formed without having a trapping pocket, a fact which indicates that the Regge pole is not necessarily associated with partial-wave-orbiting resonances.

We plotted in Fig. 11 the cross section σ_P (short-dashed line), σ_B (long-dashed line), and σ_T (thin-solid line) for the E18 potential, just as we did for the LC potential in Fig. 8. As is expected, the pole term does not show the resonance character in the angular distribution, and the behavior of σ_P and σ_B is very similar to what it was in Fig. 8(b). Nevertheless, the resultant σ_T here is quite different from that in Fig. 8. The cancellation between σ_P and σ_T here must be much more delicate than it was in Fig. 8(b). For the sake of comparison, we also reproduced in Fig. 11 the cross sections which were given in Ref. 1, obtained by the one-pole-plus-background parametrization method, and also the cross section of the pole term only in the parametrization method.

Here we define the pole (background) amplitude $f_P(\theta)$ ($f_B(\theta)$) in the parametrization method by

$$f_B(\theta) = f_C(\theta) + \frac{1}{2ik}\sum_l (2l+1)e^{2i\sigma_l}[\eta_B(l)-1]P_l(\cos\theta)\,, \tag{10a}$$

$$f_P(\theta) = \frac{1}{2ik}\sum_l (2l+1)e^{2i\sigma_l}\eta_P(l)P_l(\cos\theta)\,, \tag{10b}$$

where

$$\eta_B(l) = S_l^0\,, \tag{11a}$$

$$\eta_P(l) = \frac{iD(l)S_l^0}{l - l_0 - i\Gamma(l)/2}\,, \tag{11b}$$

with the notations of Ref. 1. In Fig. 11, the thin solid line, dot-dashed line, and thick solid line correspond to $\sigma_B(\theta) = |f_B(\theta)|^2$, $\sigma_P(\theta) = |f_P(\theta)|^2$, and $\sigma(\theta)$

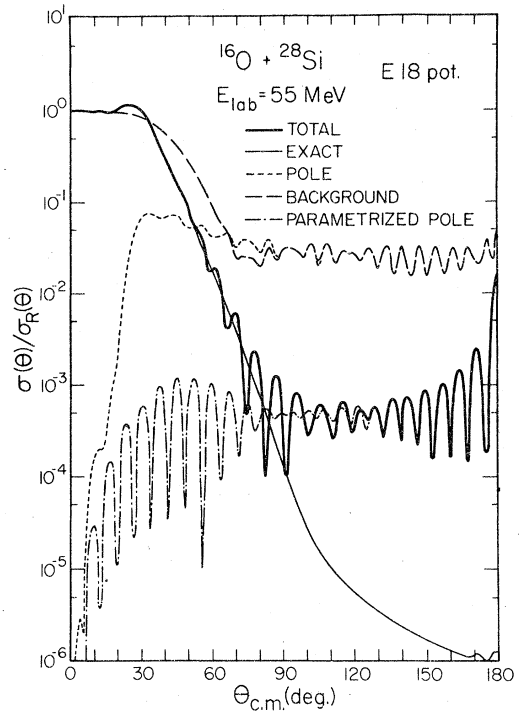

FIG. 11. Pole and background decomposition of the angular distribution in E18 potential both in the exact calculation and the one-pole-plus-background parametrization (Ref. 1.). The short (long) dashed line corresponds to the pole (background) contribution to the σ_T (thin solid line) in the exact calculation. The dot-dashed (the thin-solid) line corresponds to the angular distribution in the pole (background) term in the one-pole-plus-background approximation and the thick solid line gives the total angular distribution obtained by the coherent superposition of the pole and background terms in this approximation. Note that all the cross sections plotted are divided by σ_{Ruth}.

$= |f_B(\theta) + f_P(\theta)|^2$, respectively, in the parametrization method. As is expected, there is a large difference between the σ_P obtained exactly and that obtained by parametrization. The former is associated with the E18 potential, but the latter is entirely *ad hoc*. We shall discuss in the next section a possible way to improve the use of a parametrized pole, if one so chooses.

IV. SUMMARY AND DISCUSSION

Studies were made in detail of the properties of the Regge poles and the accompanying background integrals. They were derived rigorously from the several optical model potentials that gave good fits to the data of Braun-Munzinger *et al.*[1] and were thus considered realistic. A similar analysis had been made earlier in TW,[8] but the present analysis produced a few features which were not encountered there. We believe this dif-

ference originated from the fact that we use here potentials[4-6] whose real parts are much deeper than those used in TW. The deep real potential results in a greatly increased number of Regge poles, appearing in the first quadrant of the complex angular momentum plane. Most of these poles have similar strengths and are packed very closely together. This fact all but prohibits one from singling out the effect of any one pole, which was possible with a shallower potential at sufficiently high $E_{\text{c.m.}}$.[8]

The use of deep real potentials is a comparatively new trend employed in the optical model analyses of the scattering of heavy ions, and we believe that this is a correct approach. The results of the present study may thus be taken as a warning against attempts to fit data by introducing, rather than deriving, a Regge pole and parametrizing it in an *ad hoc* way. As we have exemplified in the inset of Fig. 9, it is of course technically possible to single out the contribution of a Regge pole, so that a sharp peak appears in $|C_l^P|$ considered as a function of l. As was seen in Fig. 9, however, this sharp peak does not result in a dominance of the pole term in determining the angular distribution at large angles. In the phenomenological Regge-pole analysis,[1,3] the pole term contributes exclusively to the angular distribution at large angles, which the background term dominates the forward angular distribution.

One may still find it useful to use a parametrized Regge-pole method. In that case, we want to recommend the following method. Take a realistic optical potential, and calculate first C_l in the standard optical model calculation. A parametrized Regge-pole term C_l^P may then be introduced, and C_l^B is obtained by subtracting C_l^P from C_l. This method allows one to avoid parametrizing C_l^P and C_l^B separately, for which there seems to exist no known guiding principle.

The data of Braun-Munzinger *et al.*[1,12] also include the angular distribution to excite inelastically the 2_1^+ state in ^{28}Si, and further the excitation function of the 180° cross section of the elastic scattering. The angular distribution of the 2_1^+ state also shows strong oscillation and a large backward rise, which would require one to use the coupled-channel method, rather than the DWBA method, to fit. Although the LC potential reproduces nicely the envelope of the excitation function,[6] it does not reproduce sufficiently well the oscillation, particularly at large E_{lab}. This trouble might be removed by the use of the coupled-channel method.[13]

Suppose that such a coupled-channel fit is made successfully. From the point of view of the content of the present paper, it might be of great interest to perform a similar analysis based on coupled-channel equations. Both in TW and in the present paper we solved an uncoupled equation, i.e., Eq. (4). That a similar calculation can be done for the simplest set of coupled equations is already known,[14] however. Such a calculation will be the subject of our future work.

We are very much indebted to Dr. D. Dehnhard, Dr. V. Shkolnik, Dr. M. Golin, Dr. S. Kahana, Dr. S. Y. Lee, and Dr. Y-d. Chan, who so generously informed us of the results of their search of optical model parameters, without which the present work could not have been even attempted. Useful discussions and comments made by Dr. T. Udagawa and Dr. W. R. Coker are also highly appreciated. The present work was partly supported by the U. S. Department of Energy.

---

*On leave from Department of Physics, University of Saga, Saga 840, Japan.

[1]P. Braun-Munzinger, G. M. Berkowitz, T. M. Cormier, C. M. Jachcinski, J. W. Harris, J. Barrette, and M. J. LeVine, Phys. Rev. Lett. 38, 944 (1977).

[2]J. G. Cramer, R. M. DeVries, D. A. Golberg, M. S. Zisman, and C. F. Maguire, Phys. Rev. C 14, 2158 (1976).

[3]K. W. McVoy, Phys. Rev. C 3, 1104 (1971).

[4]V. Shkolnik and D. Dehnhard, private communication; D. Dehnhard, invited talk at the Symposium on Heavy Ion Elastic Scattering, University of Rochester, 1977 (unpublished).

[5]M. Golin and S. Kahana, private communication; S. Kahana, invited talk at the Symposium on Heavy Ion Elastic Scattering, University of Rochester, 1977 (unpublished).

[6]S. Y. Lee, private communication; S. Y. Lee and Y-d. Chan, University of Washington. Report No. RLO-1388-743, 1977 (unpublished).

[7]See, for example, R. G. Newton, *The Complex j-plane* (Benjamin, New York, 1964).

[8]T. Tamura and H. H. Wolter, Phys. Rev. C 6, 1976 (1972).

[9]T. Regge, Nuovo Cimento 14, 951 (1959); A. Bottino, A. M. Longoni, and T. Regge, *ibid.* 23, 954 (1962).

[10]D. M. Brink and N. Takigawa, Nucl. Phys. A279, 159 (1977).

[11]N. Takigawa and S. Y. Lee, Nucl. Phys. A292, 173 (1977); S. Y. Lee, Orsay Report No. IPNO/TH 77-48, 1977 (unpublished).

[12]P. Braun-Munzinger and J. Barrette, invited talk at Symposium on Heavy Ion Elastic Scattering, University of Rochester, 1977 (unpublished).

[13]T. Tamura, Rev. Mod. Phys. 37, 679 (1965); S. Okai and T. Tamura, Nucl. Phys. 31, 185 (1962).

[14]C. Dullemont and E. van Beveren, Ann. Phys. N. Y. 105, 318 (1977).